Electrodeposition of silver nanoparticles in presence of different complexing agents by time-resolved Raman spectroelectrochemistry.

D. Ibañez[1,], D. Izquierdo[1], C. Fernandez-Blanco[2], A. Heras[1], A. Colina[1].*

1. Department of Chemistry, Universidad de Burgos, Pza. Misael Bañuelos s/n, 09001, Burgos, Spain.

2. Group UVaSens, Dpt. Inorganic Chemistry, Engineers School, Universidad de Valladolid, Valladolid, Spain.

* Corresponding author: dibanez@ubu.es, Tel: +34 947 258817, Fax: +34 947 258831.

Abstract

Chemical and physical properties of metal nanoparticles (NPs) are determined not only by the synthesis method used to prepare them, but also by the experimental conditions under the generation process takes place. One of the most important factors in the synthesis of NPs is the presence of complexing agents in the media that can change the size and shape of the NPs. The significant role of different complexing agents (cyanide, ethylenediaminetetraacetic acid and ethylenediamine) in the electrochemical formation of silver nanoparticles (AgNPs) has been analyzed by time-resolved Raman spectroelectrochemistry. Electrochemical and spectroscopic responses, obtained simultaneously, provide suitable information about the changes that occur on the platinum electrode surface during the AgNPs electrodeposition. The morphology of AgNPs has been analyzed by UV-Vis absorption spectroelectrochemistry, providing additional information and a detailed view of the electrodeposition process. The influence of the complexing agent used to generate AgNPs has been studied analyzing the surface-enhanced Raman scattering (SERS) effect of the modified substrate. Raman spectra show different SERS behaviour depending on the complexing agent and therefore, on the AgNPs generated. The relationship between SERS signals and the morphology of AgNPs has been displayed by SEM images. Time-resolved Raman spectroelectrochemistry confirms that chemical mechanism is necessary for SERS effect.

Keywords: Silver nanoparticles; SERS; Raman spectroelectrochemistry; complexing agents, UV-Vis absorption spectroelectrochemistry.

1. Introduction

Metal NPs exhibit a large range of optical, chemical, catalytic, electrical and magnetic properties due to finite size effects, making them really useful in completely different fields.[1–8] These properties can change as function of the metal, size, shape or number of components of the NPs and are different from the bulk or their constituents because the surface of the NPs are structurally and compositionally different.[9] Synthesis of metal NPs can be accomplished by different methods, such as chemical reduction,[10,11] seed-mediated,[12] photochemical,[13] electrochemical,[14,15] sonochemical,[16] lithography,[17,18] galvanic replacement,[19] thermal evaporation,[20] radiolysis, [21] sol-gel,[22] laser ablation,[23,24] chemical vapor deposition,[25] microwave assisted[26] and biological assisted.[27,28] The selection of the synthesis method, concentration of the reagents and other experimental parameters such as pH, temperature, etc., allows us to obtain NPs with specific size and shape. The control of all these factors determines the particular chemical and physical properties of the obtained NPs. In particular, electrochemical method enables the control of the deposition process, as the manner that slight changes of intensity current, applied potential, electrodeposition time, electrode material, kind or concentration of supporting electrolyte or salt precursor electrolyte can produce significant modifications in the properties of generated NPs.

In the specific case of AgNPs, there is a substantial literature on their catalytic,[29] electrochemical,[30] optical[31] and antimicrobial[32] properties that make them particularly interesting in catalysis, electronic and sensors fields.[33–36] Although the synthesis of AgNPs has been studied in the presence of several complexing ligands,[37,38] Raman spectroelectrochemistry offers a unique factor in the *in-situ* study of this process due to SERS effect is closely related to the properties of the substrate generated, an aspect that can determine the usefulness of AgNPs as

a SERS substrate.[39–45] Taking into account that Raman spectroscopy is one of the most powerful techniques in the detection and characterization of a huge variety of systems,[46–50] the combination of this spectroscopic technique with an electrochemical response provides information of different nature in a unique experiment. Furthermore, UV-Vis absorption spectroelectrochemistry is one of the few techniques that allows the *in-situ* study of the electrogeneration of metal NPs.[51,52]

In this work, the role of different complexing agents (cyanide, ethylenediaminetetraacetic acid and ethylenediamine) in the electrogeneration of AgNPs has been analyzed. SERS effect of AgNPs formed by cyclic voltammetry in presence of these markers has been studied by time-resolved Raman spectroelectrochemistry. This technique provides dynamic information that allows us to understand the processes that occur on the electrode surface during the whole experiment, and not only at selected potentials. Furthermore, combination and comparison of Raman and UV-Vis absorption spectroelectrochemistry data offer a more detailed view of the electrodeposition process, the morphology of AgNPs electrogenerated as well as SERS effect produced by the nanostructures formed on the electrode surface.

2. Material and methods

2.1. Reagents

Silver nitrate ($AgNO_3$, Aldrich), potassium cyanide (KCN, Panreac), ethylenediamine (en, Merck), ethylenediaminetetraacetic acid (EDTA, Merck) and potassium nitrate (KNO_3, Merck) as supporting electrolyte, were used as received. All chemicals were analytical grade. Aqueous solutions were freshly prepared using ultrapure water (18.2 MΩ cm resistivity at 25 °C, Milli-Q Direct 8, Millipore).

2.2. Instrumentation

All electrochemical measurements were carried out at room temperature using a potentiostat/galvanostat AUTOLAB PGSTAT 20 electrochemical system. A standard three-electrode cell was used in all experiments, consisting of a Pt working electrode (WE), a Pt wire as counter electrode (CE) and a homemade Ag/AgCl/KCl (3 M) as reference electrode (RE). Before Ag electrodeposition, the Pt working electrode was polished to a mirror finish using alumina slurries with different powder size down to 0.5 μm. Next, the electrode was thoroughly rinsed with ultrapure water and sonicated in ultrapure water in an ultrasonic bath for 15 min to remove any absorbed substances on the electrode surface.

Raman spectroelectrochemical cell, illustrated in Figure S1a (Supporting Information), consists of four pieces and two O-rings. (1) The piece placed at the bottom is used to support the WE, (2) an O-ring helps to place the WE and it avoids leakages of the solution, (3) a second piece has a hole of 6.40 mm diameter and a small recess for the placement of (4) another O-ring that prevents a possible leakage of the solution. (5) The third piece has a hole of 18.50 mm diameter and contains the bulk solution. Finally, (6) the last piece placed on the top of the cell as optical window has four small holes of 2.20 mm diameter for the placement of RE and CE, to facilitate the filling and emptying of the cell and to deoxygenate the solution if it was required. This design of the cell also guarantees the flatness of the solution needed for Raman measurements. Raman spectra were obtained using a Confocal Raman Voyage (BWTEK). A laser wavelength of 532 nm with a power of 5 mW was employed to obtain the spectra, using a 20× objective. Figure S1b (Supporting Information) displays the experimental Raman spectroelectrochemical setup, in which Confocal Raman Voyage (BWTEK) and AUTOLAB

PGSTAT 20 are synchronized by a trigger. Further details about the dynamic spectroelectrochemical Raman system have been previously reported.[51,53] An XYZ piezoelectric positioner (Newport 271) controlled by a Newport motion controller (Newport, ESP 301) was used to focus the laser beam with micrometric resolution.

Figure S2a (Supporting Information) shows UV-Vis absorption spectroelectrochemical cell used in this work. As can be noticed, Raman and UV-Vis absorption spectroelectrochemical cells are similar, and the difference is observed in the piece (6) located in the top of the cell. In the UV-Vis spectroelectrochemical case, this piece is used for the placement of the optical fiber in normal configuration and is not an optical window. Experimental UV-Vis absorption spectroelectrochemical setup, Figure S2a (Supporting Information), consists of a QE65000 Spectrometer (Ocean Optics) made up of a 1044×64 element diode array synchronized with the AUTOLAB PGSTAT 20 potentiostat. The light beam, supplied by a deuterium-halogen light source (Avalight-DH-S, Avantes) was both conducted to and collected from the spectroelectrochemical cell by a reflection probe (RP-200-7-UV-Vis, Ocean Optics). The reflection probe was a bifurcated bundle consisting of six illumination fibers around one central read fiber. UV-Vis absorption measurements were carried out in a near-normal reflection configuration where the incident beam was perpendicular to the electrode surface and the reflected light was collected by the central read fiber of the reflection probe and conducted to the spectrometer.

Scanning electron microscopy (SEM) was performed using ESEM QUANT 200FEG microscope.

3. Results and Discussion

Different complexing agents were selected to study their influence in the AgNPs electrogeneration process. Raman and UV-Vis absorption spectroelectrochemistry allow us to observe the changes of the surface morphology during the metal electrodeposition. Three complexing agents, with different stabilities of their Ag-complexes were selected, in particular cyanide (CN^-), ethylenediaminetetraacetic acid (EDTA) and ethylenediamine (en). In order to study the silver reduction potential a linear voltammetry was performed in an aqueous solution that contains 4.8×10^{-3} M $AgNO_3$, 0.4 M KNO_3 as supporting electrolyte and 2.8×10^{-2} M of complexing agent. Figure 1 shows the reduction linear voltammograms of Ag^+ in presence of different complexing agent. A blank experiment was carried out in a complexing agent free solution (blue line Figure 1). In this case, Ag^+ reduction occurs around +0.33 V. The presence of EDTA in the silver solution produces a slightly change in the reduction potential respect to the Ag^+ reduction in absence of complexing agent solution, and this process is observed at lower potential (+0.28 V, orange line Figure 1). Although the reduction potential of Ag^+ decreases to -0.03 V in presence of ethylenediamine (yellow line Figure 1), the most pronounced change takes place in presence of CN^- (purple line in Figure 1). In this last case, Ag^+ reduction occurs around -0.77 V, a potential significantly lower than those reported in the previous experiments.

Therefore, data extracted from Figure 1 indicate that the most stable complexes are obtained when CN^- ions are present in the solution. An intermediate case occurs with ethylenediamine while the Ag-EDTA complex shows the lowest stability. Comparison of the stability constants of these three complexes agrees with the results and the conclusions above explained, being the Ag-CN^- complexes formation constants the highest ($\beta_2 = 1.26\times10^{21}$, $\beta_3 = 5.01\times10^{21}$, $\beta_4 = 3.98\times10^{20}$),

intermediate values for Ag-ethylenediamine complexes ($\beta_1 = 5.01\times10^4$, $\beta_2 = 5.01\times10^7$) and the lowest for Ag-EDTA complex ($\beta_1 = 2.09\times10^7$).[54]

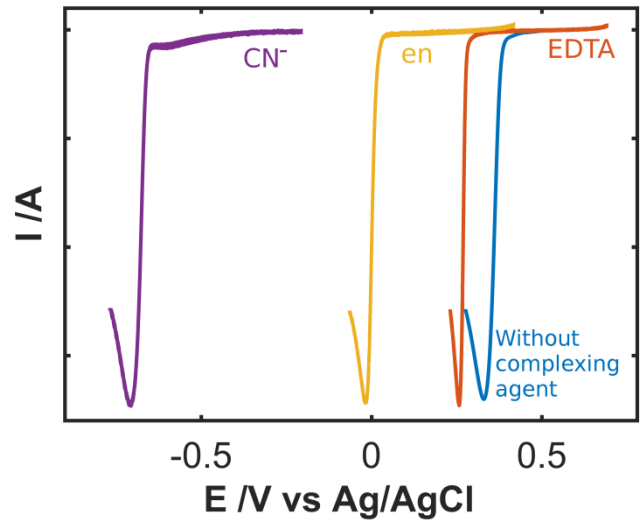

Figure 1. Electrochemical Ag^+ reduction in presence of different complexing agents, CN^- (purple line), ethylenediamine (yellow line), and EDTA (orange line). A linear voltammetry was performed in 4.8×10^{-3} M $AgNO_3$, 0.4 M KNO_3 and 2.8×10^{-2} M of complexing agent solution. A blank experiment was performed without complexing agent in the solution (blue line). Scan rate: 0.01 V s^{-1}.

3.1. AgNPs electrodeposition in presence of cyanide.

The electrodeposition of AgNPs in presence of cyanide was previously studied by time-resolved Raman and UV-Vis absorption spectroelectrochemistry.[51] Here, we show similar results in order to understand the relationship between Raman and UV-Vis responses and to compare the role of different complexing agents in SERS effect.

AgNPs electrodeposition and their redissolution was performed by cyclic voltammetry, scanning the potential from 0.00 V to -1.00 V and back to 0.00 V at a scan rate of 0.01 V s^{-1} in a 4.8×10^{-3} M $AgNO_3$ solution that contains 0.4 M KNO_3 as supporting electrolyte and 2.8×10^{-2} M KCN as complexing agent. As can be noticed in Figure 2, cyclic voltammogram shows a very small reduction peak around -0.60 V during the cathodic scan, which could be related to the silver underpotential deposition. However, the highest reduction peak is observed at -0.77 V, when Ag^+ in solution is reduced. In the anodic scan, the voltammogram shows a broad anodic peak around -0.48 V related to the oxidation of AgNPs.

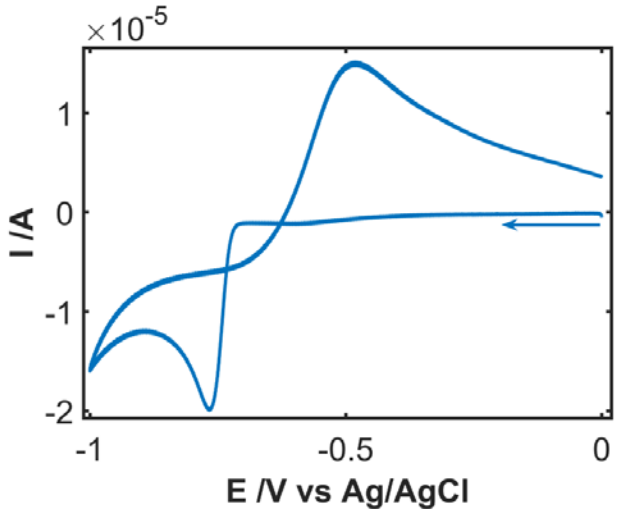

Figure 2. Cyclic voltammogram performed in $AgNO_3$ 4.8×10^{-3} M, KCN 2.8×10^{-2} M and KNO_3 0.4 M solution. The potential was scanned from 0.00 V to -1.00 V and back to 0.00 V at 0.01 V s^{-1}.

Figure 3a displays Raman spectra recorded during the forward scan of the cyclic voltammetry. A strong vibrational band at 2110 cm^{-1} related to C≡N frequency vibration, υ(C≡N),[55,56] emerges during the reduction process. Time-resolved Raman spectroelectrochemistry allow us to analyze the evolution of the υ(C≡N) band with potential (Figure 3b) during the electrodeposition experiment. Figure 3b shows that cyanide Raman band

is not observed from 0.00 V to -0.60 V due to AgNPs formation does not start, and therefore, SERS substrate is not generated. At -0.62 V Ag^+ reduction starts, SERS substrate is formed and consequently, Raman intensity of CN^- band increases. The intensity of this band increases at negative potentials, reaching a maximum at the end of the forward scan. During the backward scan, the intensity decreases from -1.00 V to -0.78 V because the properties of the AgNPs generated are changing, and SERS substrate is modified. From -0.78 V to -0.60 V, Raman intensity increases due to the metal substrate acquires better characteristics for SERS effect. However, from -0.60 V downwards the intensity of the band decreases abruptly due to the oxidation and redissolution of AgNPs.

The same experiment was carried out by time-resolved UV-Vis absorption spectroelectrochemistry, allowing us to study the characteristic plasmon band of AgNPs. Figure 3c shows UV-Vis absorption spectra recorded during the electrogeneration of AgNPs on the electrode surface. From 0.00 V to -0.80 V (Figure 3c) a broad plasmon band centered on 520 nm begins to grow indicating that polydispersed spherical NPs are growing. At more negative potentials than -0.80 V, two different plasmon bands are distinguished, one centered at 430 nm, related to the transversal dipole resonance and another that red-shifts with potential due to the longitudinal dipole resonance,[57] indicating not only a change in size but also in shape of NPs. From the shape of the plasmon band at -1.00 V (green line in Figure 3c) and evolution of plasmon band at 430 nm with potential (Figure 3d), we suggest that AgNPs changes from spherical shape to other different asymmetrical shape.[58,59] Furthermore, comparison of evolution of Raman band at 2110 cm^{-1} (Figure 3b) and UV-Vis band at 430 nm (Figure 3d) with potential shows that during the electrodeposition/redissolution process the two signals are related but their behaviors do not match exactly. Initially, neither Raman nor plasmon band are

distinguished in the respective spectra. Cyanide Raman band begins to grow at -0.62 V when the first reduction process takes places (Figure 2). On the other hand, UV-Vis plasmon band increases at more negative potential, around -0.75 V. Hence, the first reduction process observed at -0.60 V in the cathodic scan (Figure 2) produces the deposition of very small AgNPs without plasmon band but with enough SERS properties to provide the enhanced cyanide Raman band.

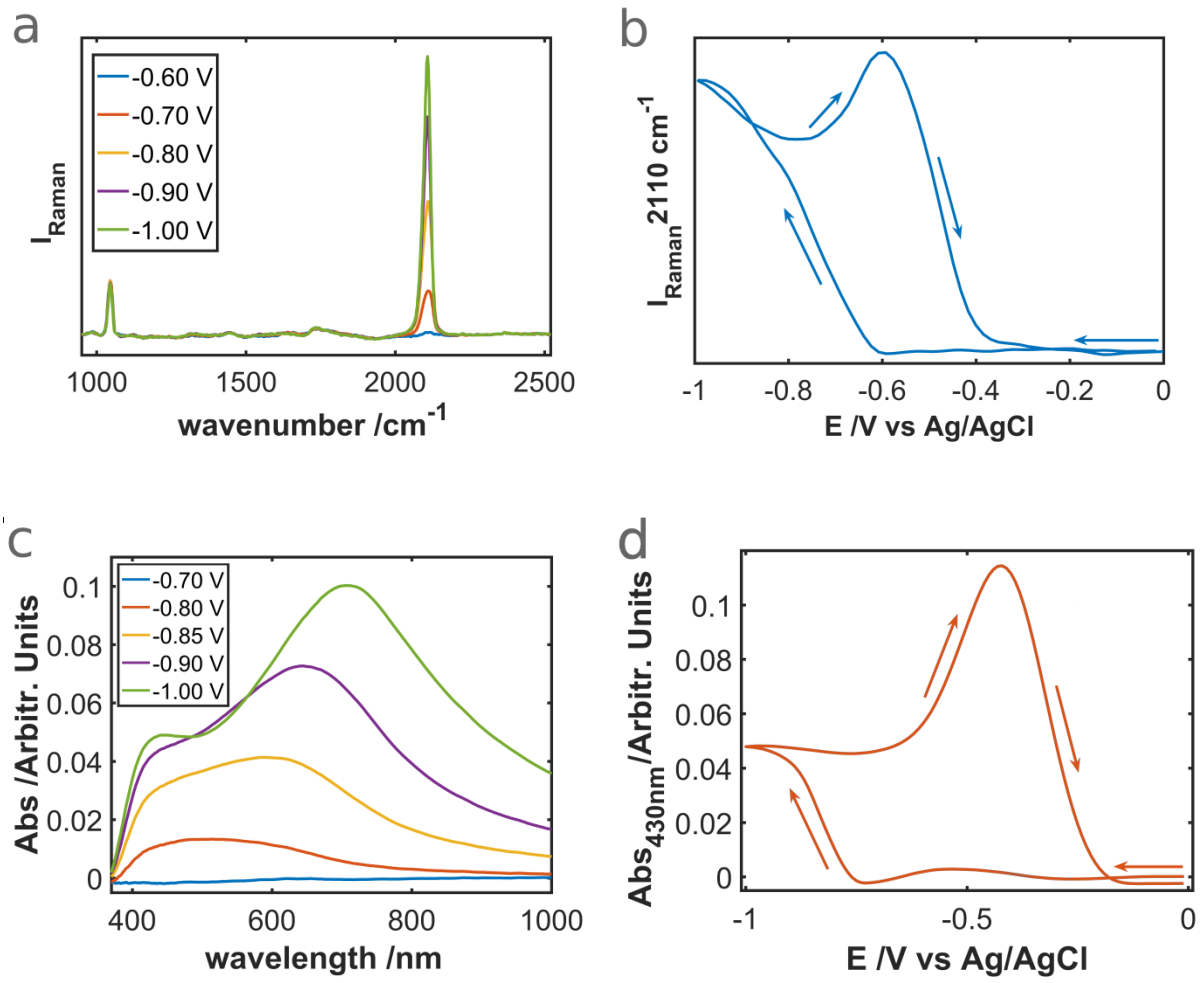

Figure 3. (a) Raman spectra recorded during the forward scan, integration time: 1600 ms. (b) Evolution of Raman intensity band at 2110 cm^{-1} with potential. (c) UV-Vis absorption spectra recorded during the forward scan. (d) Evolution of UV-Vis band at 430 nm with potential. Experimental conditions as in Figure 2.

Figure S3 (Supporting Information) displays UV-Vis spectra recorded during the backward scan (Figure S3a) and evolution of maximum of plasmon band with potential (Figure S3b). Comparison of Figure 3d and Figure S3 (Supporting Information) provides more information of the spectroelectrochemical behaviour during the electrochemical generation and redissolution of AgNPs. In the backward scan, from -1.00 V to -0.60 V, the maximum of the plasmon band moves fast to longer wavelengths, indicating a change in NPs shape. At -0.48 V the band centered at longer wavelengths is blue-shifted and the intensity decreases to obtain only one band at 430 nm related to spherical AgNPs. Finally, as can be noticed in Figure S3a (Supporting Information), from -0.40 V to 0.00 V the redissolution of AgNPs takes place and the band centered at 430 nm vanishes.

During the electrodeposition of silver in presence of cyanide, the evolution of Raman spectra with the composition of the solution is particularly interesting. Electrodeposition of AgNPs was performed by cyclic voltammetry, scanning the potential from 0.00 V to −1.00 V and back to 0.00 V at a scan rate of 0.01 V s^{-1} in an aqueous solution that contains 4.8×10^{-3} M $AgNO_3$, 0.4 M KNO_3 and different concentration of KCN (from 2.8×10^{-2} M to 2.8×10^{-11} M). Figure 4 shows Raman spectra recorded when the highest SERS effect for the cyanide band is observed during the electrodeposition process. Figure 4 demonstrates that the intensity and position of the υ(C≡N) Raman band depends on the cyanide concentration and thus, on the AgNPs generated on the electrode surface. Chemistry of Ag-CN^- establishes the formation of different complexes: [51,60]

$$Ag^+ + CN^- \leftrightarrows AgCN \qquad \upsilon_{Raman}= 2164\text{-}2167\ cm^{-1} \qquad \text{(eq. 1)}$$

$$Ag^+ + 2CN^- \leftrightarrows Ag(CN)_2^- \qquad \upsilon_{Raman}= 2135\text{-}2145\ cm^{-1} \qquad \text{(eq. 2)}$$

$$Ag(CN)_2^- + CN^- \leftrightarrows Ag(CN)_3^{2-} \qquad \upsilon_{Raman} = 2105\text{-}2110\ cm^{-1} \qquad \text{(eq. 3)}$$

$$Ag(CN)_3^{2-} + CN^- \leftrightarrows Ag(CN)_4^{3-} \qquad \upsilon_{Raman} = 2090\text{-}2100\ cm^{-1} \qquad \text{(eq. 4)}$$

As can be noticed in Figure 4, Raman spectra are completely different depending on the cyanide concentration. For the highest cyanide concentration (2.8×10^{-2} M), a strong vibrational band around 2110 cm^{-1} is observed (purple line in Figure 4), corresponding to the most stable complex, $Ag(CN)_4^{3-}$ (eq. 4). According to previous work,[51] a clear red-shifting of this cyanide band is observed when the concentration of cyanide is lowered, due to the generation of different cyanide complexes with a lower number of ligands. When cyanide concentrations were modified to 2.8×10^{-5} M and 2.8×10^{-8} M (orange and green lines in Figure 4, respectively) different complexes are distinguished. For the lowest concentration, 2.8×10^{-11} M (blue line in Figure 4), even a very weak band is detected, showing the good analytical detection limit of SERS effect. It demonstrates that the spectroelectrochemical methodology is a good candidate to control the electrosynthesis of AgNPs and hence, to obtain SERS active substrates with excellent properties.

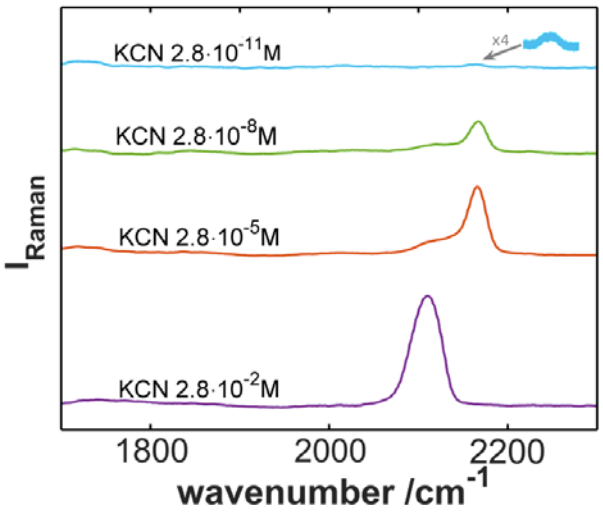

Figure 4. Raman spectra recorded when the highest SERS effect for the cyanide band is observed during AgNPs generation. AgNPs electrodeposition was performed by cyclic

voltammetry in $AgNO_3$ 4.8×10^{-3} M, 0.4 M KNO_3 and different concentration of KCN: 2.8×10^{-2} M (purple line), 2.8×10^{-5} M (orange line), 2.8×10^{-8} M (green line) and 2.8×10^{-11} M (blue line).

3.2. AgNPs electrodeposition in presence of ethylenediaminetetraacetic acid (EDTA).

AgNPs electrodeposition was also performed in presence of EDTA by cyclic voltammetry, scanning the potential from +0.75 V to 0.00 V and back to +0.75 V at a scan rate of 0.01 V s^{-1} in a 4.8×10^{-3} M $AgNO_3$ solution containing 0.4 M KNO_3 as supporting electrolyte and 2.8×10^{-2} M EDTA as complexing agent (Figure 5a). Although cyclic voltammogram is similar to the electrochemical response of AgNPs electrodeposition with cyanide, in this case the reduction peak is located at positive potentials (+0.28 V, green segment in Figure 5a) instead of at negative values. Raman spectra of Ag-EDTA complex show several bands related to different vibration modes,[61] showing all of them similar behaviour with potential. Band centered at 710 cm^{-1} is selected as representative band of Ag-EDTA complex due to its higher Raman intensity during AgNPs generation. Figure 5b displays a 3D plot Raman signal/potential/Raman Shift centered at 710 cm^{-1} obtained during the electrochemical experiment. Evolution of Raman band at 710 cm^{-1} with potential is illustrated in Figure 5c. When Ag^+ reduction starts at +0.28 V (green segment in Figure 5a) the Raman intensity of this band increases (green segment in Figure 5c), reaching a maximum of intensity at +0.28 V (purple segment in Figure 5a) during the backward scan (purple segment in Figure 5c). From this potential onwards (red segment in Figure 5a) a first oxidation step takes place, provoking the decrease of the Raman intensity (red segment in Figure 5c). After this first oxidation step, the highest oxidation peak is observed in the voltammogram (yellow segment in Figure 5a), although it does not produce changes in the Raman intensity at 710 cm^{-1} (yellow segment in Figure 5c). Hence, the loss of SERS properties of AgNPs takes

places in a first oxidation step (+0.35 V) instead of during the second and well-defined oxidation process (+0.52 V).

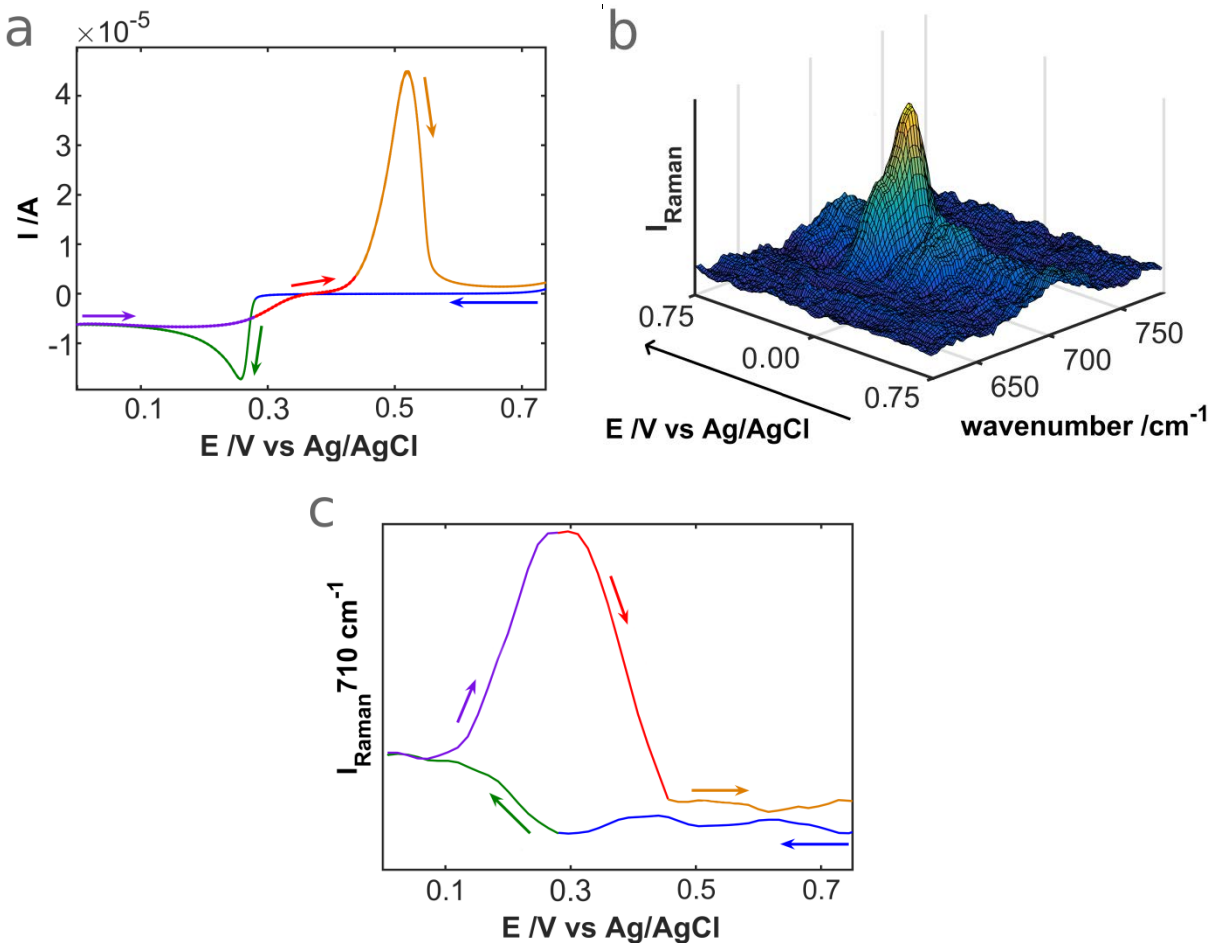

Figure 5. (a) Cyclic voltammogram performed in $AgNO_3$ 4.8×10^{-3} M, EDTA 2.8×10^{-2} M and KNO_3 0.4 M solution. The potential was scanned from +0.75 V to 0.00 V and back to +0.75 V at 0.01 V s^{-1}. (b) 3D plot Raman signal/potential/Raman Shift obtained during the electrochemical experiment. (c) Evolution of Raman intensity band at 710 cm^{-1} with potential. Integration time: 1600 ms.

In order to demonstrate that Raman band at 710 cm^{-1} is only related to Ag-EDTA complex, Figure S4 (Supporting Information) shows the comparison of this band and Raman spectra of

EDTA and KNO_3 (solid both of them). As can be observed, a width Raman band of EDTA is located at 710 cm^{-1}, while KNO_3 shows a narrow band located at 715 cm^{-1}. Although wavenumber and width of Raman band associated with Ag-EDTA complex match with band related to EDTA, bands observed in normal Raman spectra of anions can be shifted in wavenumber and broaden most notably due to changes in the surrounding environment, orientation effects in response to adsorption or a changing electric field, and due to changes in molecular bonding lengths upon adsorption onto multiple crystallographic facets of polycrystalline metal surface like AgNPs. In this way, Raman band at 710 cm^{-1} could be originated from either EDTA and/or KNO_3. In the cyanide case, we have observed a very weak band centered around 710 cm^{-1} that is not potential dependent as the band at 2110 cm^{-1} associated with cyanide complexes. Therefore, although the band centered at 710 cm^{-1} in presence of EDTA (Figure 5b) can be also assigned to the presence of KNO_3, the evolution of this band with potential (Figure 5c) demonstrates that it should correspond to Ag-EDTA complex. Moreover, chemical interaction of EDTA and AgNPs should be stronger than the one between NO_3^- and AgNPs as in the cyanide case.

Evolution of the maximum of absorbance of the plasmon band, recorded during the UV-Vis absorption spectroelectrochemical experiment, is illustrated in Figure 6. This figure shows that the maximum of the plasmon band is shifting with potential, allowing us to conclude that the properties of the AgNPs are changing during the experiment. Initially, any plasmon band is distinguished in UV-Vis spectral region (blue segment in Figure 6b). Only when the growth of AgNPs begins, around +0.28 V, a plasmon band centered at 400 nm evolves (green segment in Figure 6b). This maximum shifts from 400 nm to longer wavelengths, higher than 1000 nm, the upper limit of the wavelength range reached with the spectrophotometer, being not possible to

determine the exact value. In the backward scan, only from +0.46 V onwards, the plasmon band is centered in the visible region of the spectrum (yellow segment in Figure 6b), just when AgNPs starts to be redissolved. Finally, at the end of the anodic scan, the potential is high enough to completely oxidize AgNPs, redissolving all NPs on the electrode surface. Therefore, when AgNPs disappear, SERS effect is also extinct.

Analysing UV-Vis spectra evolution, two absorption bands are observed in presence of EDTA when SERS effect is observed, one around 400 nm and other at wavelengths longer than 1000 nm, denoting asymmetrical nanoparticles. Position and intensity of the plasmon band is potential dependent, indicating that the shape of AgNPs is changing during the electrochemical synthesis.

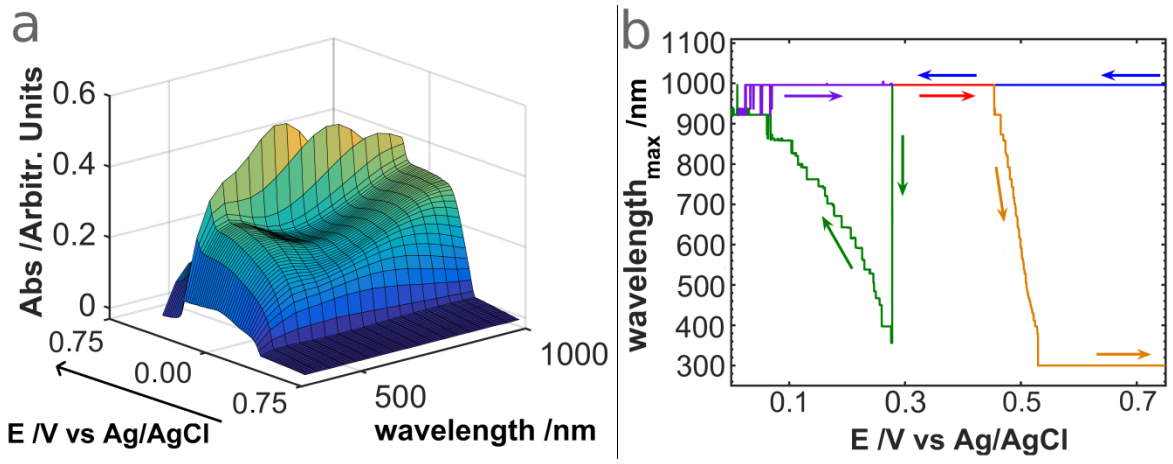

Figure 6. (a) 3D plot UV-Vis absorbance/potential/wavelength obtained during the electrochemical experiment performed in $AgNO_3$ 4.8×10^{-3} M, EDTA 2.8×10^{-2} M and KNO_3 0.4 M solution. The potential was scanned from +0.75 V to 0.00 V and back to +0.75 V at 0.01 V s^{-1}. (b) Evolution of the maximum UV-Vis wavelength of the plasmon band with the potential.

3.3. AgNPs electrodeposition in presence of ethylenediamine.

AgNPs electrosynthesis and their redissolution in presence of ethylenediamine were carried out by cyclic voltammetry, scanning the potential from +0.60 V to -0.25 V and back to +0.60 V at a scan rate of 0.01 V s^{-1} in a 4.8×10^{-3} M $AgNO_3$ solution containing 0.4 M KNO_3 as supporting electrolyte and 2.8×10^{-2} M ethylenediamine as complexing agent (Figure 7a). Although the cyclic voltammogram is similar to the electrochemical response of the AgNPs electrodeposition with CN^- and EDTA (Figure 2 and Figure 5a, respectively), the reduction peak is located at different potential (-0.03 V), as was indicated in Figure 1. Furthermore, as can be noticed in Figure 7b the spectroscopic information extracted from UV-Vis absorption spectra is completely different. Figure 7b displays the UV-Vis response during the spectroelectrochemical experiment, showing that a plasmon band around 420 nm evolves when the Ag^+ reduction takes place. However, in this media, no waveform changes with potential are observed in the plasmon band. Therefore, only spherical AgNPs are generated during this electrodeposition process and they do not show shape changes.

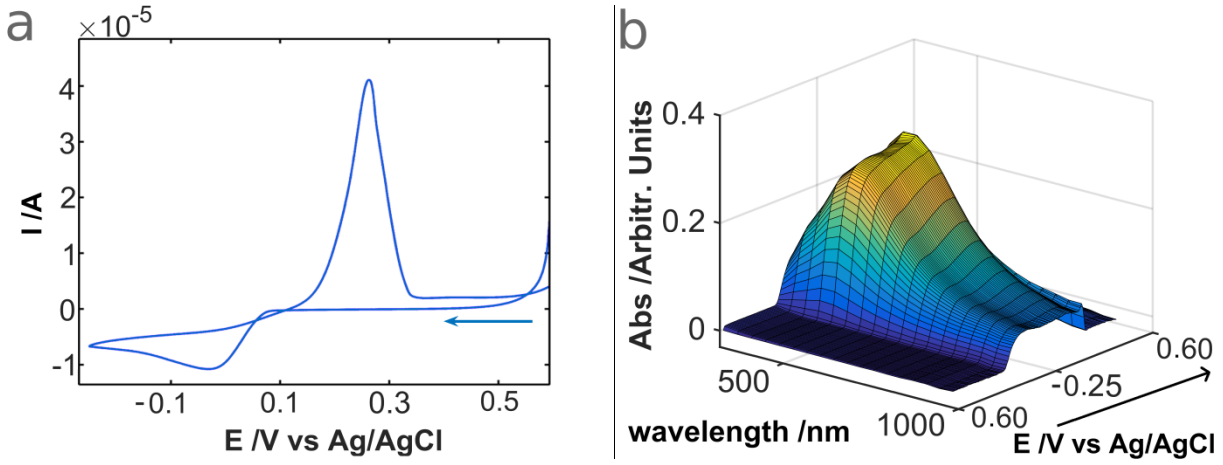

Figure 7. (a) Cyclic voltammogram performed in $AgNO_3$ 4.8×10^{-3} M, ethylenediamine 2.8×10^{-2} M and KNO_3 0.4 M solution. The potential was scanned from +0.60 V to -0.25 V and back to +0.60 V at 0.01 V s^{-1}. (b) 3D plot UV-Vis absorbance/potential/wavelength obtained during the electrochemical experiment.

Analysing the Raman spectra, surprisingly, no Raman bands of the ethylenediamine can be observed during the experiment. As can be deduced from the voltammogram and from the UV-Vis absorption spectra (Figure 7a and Figure 7b, respectively), the electrodeposition of AgNPs is guaranteed. Although a high value of absorbance is obtained, indicating that a high number of AgNPs are deposited on the electrode surface, there is not SERS effect under these experimental conditions. Therefore, we can assume that the interaction of the Ag-ethylenediamine complexes with the substrate (chemical effect) is not strong enough to observe SERS effect. This set of experiments, in an *in-situ* way during the generation of AgNPs, illustrates that not only the electromagnetic but also the chemical mechanism of SERS effect limit the enhancement of the Raman signal.

3.4. SEM characterization

In order to characterize SERS substrates, SEM images of AgNPs formed in presence of different complexing agents were performed. Analysis of several samples prepared at different deposition stages allows us to analyze their specific properties. In the cyanide case and according to previous work,[62] when the experiment has finished, the plasmon band shows a spontaneously blue-shifting band centered on 420 nm that finally vanishes because cyanide media causes the dissolution of AgNPs.[59,63,64] Hence, an *ex-situ* characterization of the NPs is not possible when experiments are finished because the metal nanostructures have changed spontaneously.

According to evolution of Raman band at 710 cm^{-1} with potential (Figure 5c), AgNPs electrogenerated in presence of EDTA were characterized by SEM at different deposition stages. Firstly, AgNPs formed by linear voltammetry from +0.75 V to 0.00 V at 0.01 V s^{-1} are shown in

Figure 8a. As can be noticed, spherical AgNPs with different size were formed (NPs from 10 nm to 90 nm are observed). Raman spectra demonstrate that spherical AgNPs generated in presence of EDTA shows SERS properties in this potential window (Figure 5c).

Furthermore, Figure 8b shows a SEM image of AgNPs electrogenerated in EDTA by cyclic voltammetry scanning the potential from +0.75 V to 0.00 V and back to +0.26 V at 0.01 V s^{-1}. The stopping potential was selected before the first oxidation process shown in Figure 5a (red segment), +0.26 V, that coincides with the maximum value of the Raman band at 710 cm^{-1}, Figure 5c. AgNPs (Figure 8b) show different shapes, not only spherical NPs are observed but also rods, triangular and amorphous AgNPs are distinguished. Comparison between Figures 8a and 8b, and the evolution of plasmon band (Figure 6b), allow us to conclude that SEM image and UV-Vis agree, because asymmetrical nanoparticles are formed. Besides, Figures 8a and 8b show another significant difference, in the second case when the potential is stopped in the backward scan (+0.26 V), AgNPs are flatter than AgNPs formed up to 0.00 V. Figure 8b demonstrates that, under the experimental conditions selected, flat AgNPs with different shapes yields better SERS response in presence of EDTA than spherical AgNPs.

Figure 8c shows a SEM image of AgNPs generated in presence of ethylenediamine when potential was scanned from +0.60 V to -0.25 V at 0.01 V s^{-1}. AgNPs obtained in presence of ethylenediamine show spherical shape with a size around 10-20 nm, but they tend to be agglomerated. It is noteworthy that around the biggest agglomerates, there are not small AgNPs, showing that most NPs generated in this area form isolated agglomerates. As was explained before, no Raman signal was observed, demonstrating that these isolated AgNPs and agglomerates, generated in presence of ethylendiamine, do not show a measureable SERS

response. In spite of the known excellent SERS properties of spherical AgNPs, this work shows that isolated agglomerates do not yield a detectable SERS response using the same experimental conditions for obtaining Raman spectra that the ones used in the electrosynthesis of AgNPs in presence of EDTA or cyanide.

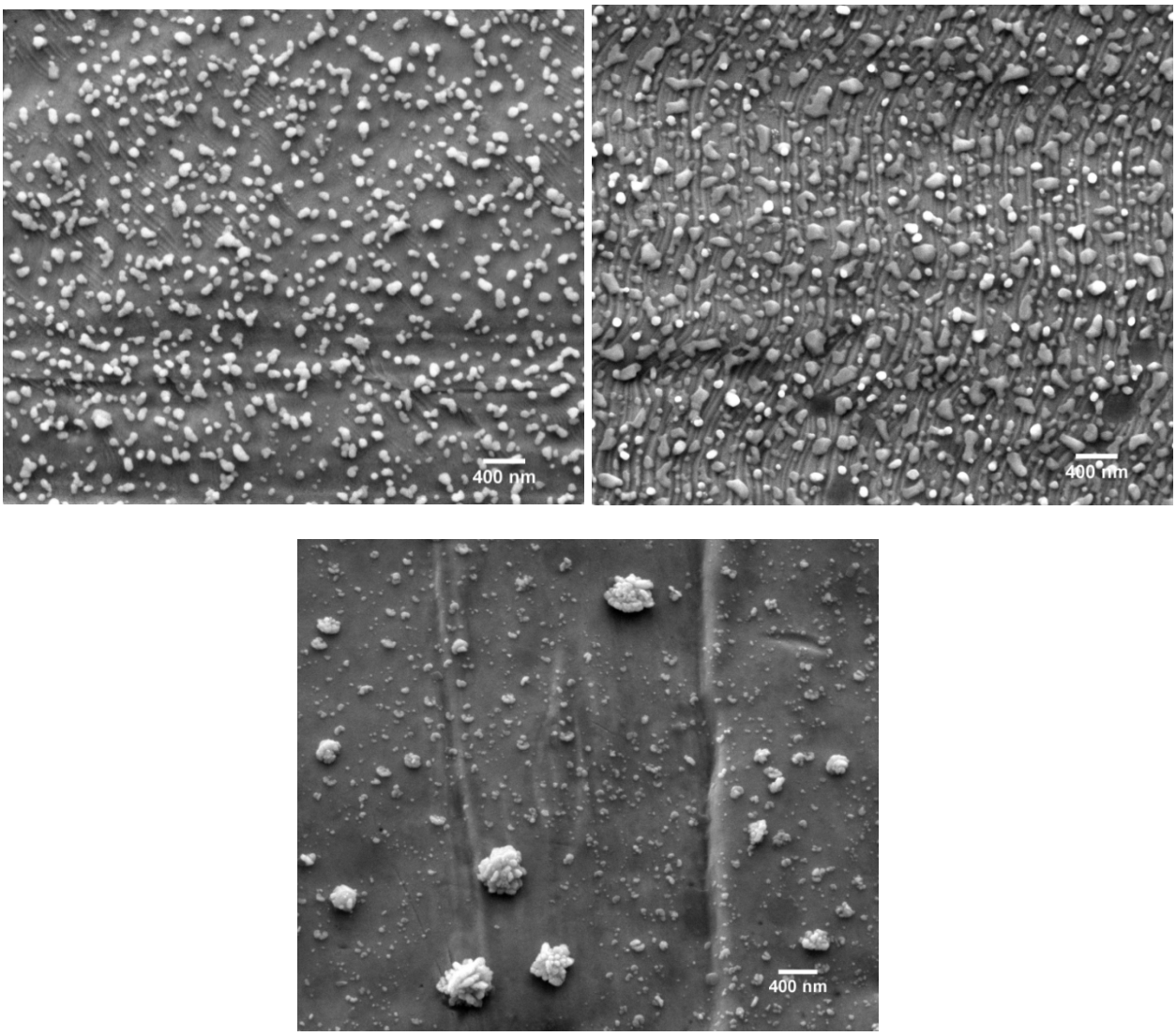

Figure 8. SEM image of AgNPs generated in presence of EDTA at different deposition stages: the potential was scanned (a) from +0.75 V to 0.00 V at 0.01 V s^{-1} and (b) from +0.75 V to 0.00 V and back to +0.26 V at 0.01 V s^{-1}. (c) SEM image of AgNPs generated in presence of ethylenediamine scanning the potential from +0.60 V to -0.25 V at 0.01 V s^{-1}.

4. Conclusions

Time-resolved Raman spectroelectrochemistry, in which the combination of two analytical instrumental techniques simultaneously provides information of different nature, has been demonstrated as a very powerful technique to the *in-situ* study of the electrogeneration of AgNPs on an electrode surface. Complementary information has been obtained by UV-Vis absorption spectroelectrochemistry, allowing us to elucidate shape changes of AgNPs generated during the whole electrochemical process and correlate them with changes in the SERS response. SERS effect of AgNPs in presence of three complexing agents (cyanide, ethylenediaminetetraacetic acid and ethylenediamine) shows different behavior, confirming that SERS effect depends on the kind of complexing agent present in the media. Cyanide, in high concentration, produces the modification of the shape of AgNPs, from spheres to other asymmetrical shapes with a higher SERS effect. However, at lower concentration of cyanide a red-shifting of the Raman band is observed due to the formation of $Ag(CN)_n^{(n-1)-}$ complexes with lower number of ligands. It is remarkable the detection limit of SERS effect when very low concentration of cyanide complexing agent is used, and even a very weak cyanide band is detected using a 2.8×10^{-11} M concentration. In EDTA case, high concentration of this agent produces changes in the shape of AgNPs during the electrodeposition process, and asymmetrical nanoparticles are generated. On the other hand, ethylenediamine only produces isolated spherical AgNPs that tend to form agglomerates that do not show a measurable SERS response, and consequently, no Raman bands related to Ag-ethylenediamine complexes are observed. Although SERS properties of AgNPs are well-known, under the experimental conditions selected in this work the specific properties of metal NPs electrogenerated (size, AgNPs spacing, dispersity, etc.) do not show detectable SERS effect. Spectroelectrochemical methodology, in particular Raman and UV-Vis absorption

spectroelectrochemical techniques, allows us to study the electrogeneration of AgNPs in presence of three complexing agents with different adsorption properties as well as the scattering cross sections. Spectroelectrochemical results lead to conclude that SERS effect depends strongly on the complexing agents present in the media, i.e, on the probe molecule analyzed. According to the results shown in this work, we confirm, using time-resolved spectroelectrochemistry, that chemical mechanism is necessary for obtaining SERS effect and only the generation of NPs is not enough to produce SERS effect.

A**cknowledgements**

Financial support from Ministerio de Economía y Competitividad (CTQ2014-61914-EXP, CTQ2014-55583-R, CTQ2015-71955-REDT) and Junta de Castilla y León (BU033-U16) is gratefully acknowledged. D. Ibañez thanks Ministerio de Economía y Competitividad for his post-doctoral fellowship (CTQ2014-61914-EXP). Parque Científico of Universidad de Valladolid and Manuel Avella are acknowledged for SEM images.

References

[1] M. A. Sanchez-Castillo, C. Couto, W. B. Kim, J. A. Dumesic, *Angew. Chemie - Int. Ed.* **2004**, *43*, 1140.

[2] M. D. Hughes, Y.-J. Xu, P. Jenkins, P. McMorn, P. Landon, D. I. Enache, A. F. Carley, G. A. Attard, G. J. Hutchings, F. King, E. H. Stitt, P. Johnston, K. Griffin, C. J. Kiely, *Nature* **2005**, *437*, 1132.

[3] Y. Horiguchi, T. Niidome, S. Yamada, N. Nakashima, Y. Niidome, *Chem. Lett.* **2007**, *36*, 952.

[4] C. S. Thaxton, C. A. Mirkin, J. Nam, *Science (80-.).* **2003**, *301*, 1884.

[5] R. Gottesman, S. Shukla, N. Perkas, L. A. Solovyov, Y. Nitzan, A. Gedanken, *Langmuir* **2011**, *27*, 720.

[6] A. Kumar, P. K. Vemula, P. M. Ajayan, G. John, *Nat. Mater.* **2008**, *7*, 236.

[7] A. Kim, F. S. Ou, D. A. A. Ohlberg, M. Hu, R. S. Williams, Z. Li, *J. Am. Chem. Soc.* **2011**, *133*, 8234.

[8] J.-S. Lee, J. Cho, C. Lee, I. Kim, J. Park, Y.-M. Kim, H. Shin, J. Lee, F. Caruso, *Nat. Nanotechnol.* **2007**, *2*, 790.

[9] T. K. Sau, A. L. Rogach, F. Jäckel, T. A. Klar, J. Feldmann, *Adv. Mater.* **2010**, *22*, 1805.

[10] N. R. Jana, *Analyst* **2003**, *128*, 954.

[11] X.-D. Tian, B.-J. Liu, J.-F. Li, Z.-L. Yang, B. Ren, Z.-Q. Tian, *J. Raman Spectrosc.* **2013**, *44*, 994.

[12] V. Sharma, K. Park, M. Srinivasarao, *Mater. Sci. Eng. R Reports* **2009**, *65*, 1.

[13] X. Huang, X. Zhou, S. Wu, Y. Wei, X. Qi, J. Zhang, F. Boey, H. Zhang, *Small* **2010**, *6*, 513.

[14] D. Ibañez, M. Galindo, A. Colina, E. Valles, A. Heras, E. Gomez, *Electrochim. Acta* **2017**,

243, 349.

[15] D. Ibañez, J. Garoz-Ruiz, D. Plana, A. Heras, D. J. Fermín, A. Colina, *Electrochim. Acta* **2016**, *217*, 262.

[16] A. Gedanken, *Ultrason. Sonochem.* **2004**, *11*, 47.

[17] M. Green, F. M. Liu, *J. Phys. Chem. B* **2003**, *107*, 13015.

[18] N. A. Abu Hatab, J. M. Oran, M. J. Sepaniak, *ACS Nano* **2008**, *2*, 377.

[19] Y. Sun, *Chem. Mater.* **2007**, *19*, 5845.

[20] M. Frank, M. Baumer, *Phys. Chem. Chem. Phys.* **2000**, *2*, 3723.

[21] B. D. Du, D. V Phu, N. N. Duy, N. T. K. Lan, V. T. K. Lang, N. V. K. Thanh, N. T. P. Phong, N. Q. Hien, *J. Exp. Nanosci.* **2008**, *3*, 207.

[22] R. Narayanan, M. A. El-Sayed, *J. Phys. Chem. B* **2005**, *109*, 12663.

[23] C. Domingo, V. Resta, S. Sanchez-Cortes, J. V. García-Ramos, J. Gonzalo, *J. Phys. Chem. C* **2007**, *111*, 8149.

[24] Q. Wang, S. Bai, Y. Zhao, Z. Liu, *Appl. Surf. Sci.* **2014**, *303*, 312.

[25] A. M. Boies, J. T. Roberts, S. L. Girshick, B. Zhang, T. Nakamura, A. Mochizuki, *Nanotechnology* **2009**, *20*, 295604.

[26] M. Tsuji, M. Hashimoto, Y. Nishizawa, M. Kubokawa, T. Tsuji, *Chem. - A Eur. J.* **2005**, *11*, 440.

[27] I. D. G. Macdonald, W. E. Smith, *Langmuir* **1996**, *12*, 706.

[28] A. R. Vilchis-Nestor, V. Sánchez-Mendieta, M. A. Camacho-López, R. M. Gómez-Espinosa, M. A. Camacho-López, J. A. Arenas-Alatorre, *Mater. Lett.* **2008**, *62*, 3103.

[29] Y. Lu, Y. Mei, M. Drechsler, M. Ballauff, *Angew. Chemie - Int. Ed.* **2006**, *45*, 813.

[30] J. Wang, O. Rincón, R. Polsky, E. Dominguez, *Electrochem. Commun.* **2003**, *5*, 83.

[31] K. L. L. Kelly, E. Coronado, L. L. L. L. Zhao, G. C. G. C. Schatz, *J. Phys. Chem. B* **2003**, *107*, 668.

[32] M. Rai, A. Yadav, A. Gade, *Biotechnol. Adv.* **2009**, *27*, 76.

[33] W. Xie, P. Qiu, C. Mao, *J. Mater. Chem.* **2011**, *21*, 5190.

[34] K. C. Bantz, A. F. Meyer, N. J. Wittenberg, H. Im, O. Kurtuluş, S. H. Lee, N. C. Lindquist, S.-H. Oh, C. L. Haynes, *Phys. Chem. Chem. Phys.* **2011**, *13*, 11551.

[35] J. N. Anker, W. P. Hall, O. Lyandres, N. C. Shah, J. Zhao, R. P. Van Duyne, *Nat. Mater.* **2008**, *7*, 442.

[36] H. Kim, K. M. Kosuda, R. P. Van Duyne, P. C. Stair, *Chem. Soc. Rev.* **2010**, *39*, 4820.

[37] R. Chadha, A. Das, N. Maiti, S. Kapoor, *Mater. Chem. Phys.* **2014**, *148*, 1124.

[38] L. Kvítek, R. Prucek, A. Panáček, R. Novotný, J. Hrbáč, R. Zbořil, *J. Mater. Chem.* **2005**, *15*, 1099.

[39] K. H. Zheng, Y. C. Chou, Y. J. Wu, Y. T. Lee, *J. Raman Spectrosc.* **2010**, *41*, 632.

[40] D. Ibañez, A. Santidrian, A. Heras, M. Kalbáč, A. Colina, *J. Phys. Chem. C* **2015**, *119*, 8191.

[41] P. P. Fang, J. F. Li, Z. L. Yang, L. M. Li, B. Ren, Z. Q. Tian, *J. Raman Spectrosc.* **2008**, *39*, 1679.

[42] G. V. P. Kumar, *J. Raman Spectrosc.* **2009**, *40*, 2069.

[43] C. Shi, W. Zhang, R. L. Birke, J. R. Lombardi, *J. Electroanal. Chem.* **1997**, *423*, 67.

[44] M. Wang, T. Spataru, J. R. Lombardi, R. L. Birke, *J. Phys. Chem. C* **2007**, *111*, 3044.

[45] J. Xu, R. L. Birke, J. R. Lombardi, *J. Am. Chem. Soc.* **1987**, *109*, 5645.

[46] M. J. Weaver, *J. Raman Spectrosc.* **2002**, *33*, 309.

[47] E. Van Elslande, S. Lecomte, A. S. Le Ho, *J. Raman Spectrosc.* **2008**, *39*, 1001.

[48] C. L. Brosseau, F. Casadio, R. P. Van Duyne, *J. Raman Spectrosc.* **2011**, *42*, 1305.

[49] C. Ruan, W. Wang, B. Gu, *J. Raman Spectrosc.* **2007**, *38*, 568.

[50] E.-O. Ganbold, J.-H. Park, U. Dembereldorj, K.-S. Ock, S.-W. Joo, *J. Raman Spectrosc.* **2011**, *42*, 1614.

[51] D. Ibañez, C. Fernandez-Blanco, A. Heras, A. Colina, *J. Phys. Chem. C* **2014**, *118*, 23426.

[52] C. Fernandez-Blanco, D. Ibañez, A. Colina, V. Ruiz, A. Heras, *Electrochim. Acta* **2014**, *145*, 139.

[53] D. Ibañez, E. C. Romero, A. Heras, A. Colina, *Electrochim. Acta* **2014**, *129*, 171.

[54] J. A. Dean, *Lange's Handbook of Chemistry*, McGraw-Hill Inc., New York, 15th edn., **1998**.

[55] B. Reents, G. Lacconi, W. Plieth, *J. Electroanal. Chem.* **1992**, *325*, 207.

[56] F. Schaaf, G. Laufer, J. T. Huneke, *Chem. Phys. Lett.* **1981**, *82*, 571.

[57] C. J. C.-J. Huang, P.-H. P. H. Chiu, Y.-H. Y. H. Wang, C. F. C.-F. Yang, *J. Colloid Interface Sci.* **2006**, *303*, 430.

[58] M. Tsuji, S. Gomi, Y. Maeda, M. Matsunaga, S. Hikino, K. Uto, T. Tsuji, H. Kawazumi, *Langmuir* **2012**, *28*, 8845.

[59] B. Tang, S. Xu, J. An, B. Zhao, J. R. Lombardi, *Phys. Chem. Chem. Phys.* **2009**, *11*, 10286.

[60] M. Fleischmann, G. Sundholm, Z. Q. Tian, *Electrochim. Acta* **1986**, *31*, 907.

[61] E. J. Baran, C. C. Wagner, M. H. Torre, *J. Braz. Chem. Soc.* **2002**, *13*, 576.

[62] D. Ibañez, C. Fernandez-Blanco, A. Heras, A. Colina, *J. Phys. Chem. C* **2014**, *118*, 23426.

[63] B.-H. Lee, M.-S. Hsu, Y.-C. Hsu, C.-W. Lo, C.-L. Huang, *J. Phys. Chem. C* **2010**, *114*, 6222.

[64] F. Fathi, M. Schlitt, D. B. Pedersen, H.-B. Kraatz, *Langmuir* **2011**, *27*, 12098.

Graphical abstract